Environmental Research 228 (2023) 115783

Contents lists available at ScienceDirect

Environmental Research

journal homepage: www.elsevier.com/locate/envres

Settling velocity of microplastic particles having regular and irregular shapes ☆

Koray Deniz Goral [a,*], Hasan Gokhan Guler [a,b], Bjarke Eltard Larsen [a], Stefan Carstensen [a], Erik Damgaard Christensen [a], Nils B. Kerpen [c], Torsten Schlurmann [c], David R. Fuhrman [a]

[a] Technical University of Denmark, Department of Civil and Mechanical Engineering, DK-2800 Kgs. Lyngby, Denmark
[b] Middle East Technical University, Department of Civil Engineering, Ocean Engineering Research Center, Cankaya, Ankara, Turkey
[c] Ludwig-Franzius-Institute for Hydraulic, Estuarine and Coastal Engineering, Leibniz University Hannover, Hannover, Germany

ARTICLE INFO

Keywords:
Non-buoyant
Microplastic particles
Settling velocity

ABSTRACT

The settling velocities of 66 microplastic particle groups, having both regular (58) and irregular (eight) shapes, are measured experimentally. Regular shapes considered include: spheres, cylinders, disks, square plates, cubes, other cuboids (square and rectangular prisms), tetrahedrons, and fibers. The experiments generally consider Reynolds numbers greater than 10^2, extending the predominant range covered by previous studies. The present data is combined with an extensive data set from the literature, and the settling velocities are systematically analyzed on a shape-by-shape basis. Novel parameterizations and predictive drag coefficient formulations are developed for both regular and irregular particle shapes, properly accounting for preferential settling orientation. These are shown to be more accurate than the best existing predictive formulation from the literature. The developed method for predicting the settling velocity of irregularly-shaped microplastic particles is demonstrated to be equally well suited for natural sediments in the Appendix.

1. Introduction

Tremendous volumes of plastic waste can unfortunately now be found in aquatic environments (see e.g. Barnes et al., 2009; Browne et al., 2011; Cozar et al., 2014; Nerland et al., 2014; Jambeck et al., 2015; van Sebille et al., 2015; Lamb et al., 2018; Peeken et al., 2018; Wieczorek et al., 2018). Microplastic particles correspond specifically to those fractions having length scales less than 5 mm. If not properly disposed of, due to natural run-off processes, the long-term destination of these pollutants is often the marine environment. Due to their small size, they are easily ingested by a variety of organisms spanning the food chain, and hence may even pose a threat to human health (Law and Thompson, 2014). Understanding the long-term transport patterns and fate of microplastics in marine environments requires fundamental understanding of their basic transport properties. This includes their settling velocity, which is a commonly required basic input into more advanced transport models and parameterizations.

Several experimental studies on the settling velocity of microplastic particles have been published in recent years. The variety of regularly- and irregularly-shaped particles considered to date is summarized in Table 1. Of these, Kowalski et al. (2016) studied settling velocities of spheres, cylinders, and irregularly-shaped microplastic particles, under varying water salinity and aging factors (exposure to UV irradiation and mechanical stress). They unsurprisingly found that shape has a great influence on the settling process. They indicated strong deviations between their measurements with predictions based on the method of Dietrich (1982), designed for natural sediments. Khatmullina and Isachenko (2017) measured the settling velocities of hand-made polycaprolactone (PCL) spheres, short PCL cylinders, and fibers (fishing line cuts). They compared their settling velocity measurements with those estimated from several different methods, e.g. those of Dietrich (1982), Soulsby (1997), and Ahrens (2000), again based on data for natural sediments. They proposed their own formula to specifically calculate the settling velocities of fishing line cut fibers. Waldschläger and Schüttrumpf (2019) performed additional experiments with microplastic spheres, pellets (characterized as cylinders in Table 1), fibers, and fragments to measure both their settling and rise velocities. They similarly compared their measured results with those estimated from several

☆ Handling Editor: Aijie Wang.
* Corresponding author.
E-mail address: kdego@dtu.dk (K.D. Goral).

https://doi.org/10.1016/j.envres.2023.115783
Received 10 January 2023; Received in revised form 17 March 2023; Accepted 26 March 2023
Available online 5 April 2023

Table 1
Summary of shapes considered in previous experimental investigations on the settling velocity of microplastic particles, in addition to the present work. Note that the settling velocities for (18) particle groups reported by Guler et al. (2022) correspond to a sub-set of those measured in the present work.

Reference	Spheres	Cylinders	Disks	Plates	Cubes	Cuboids	Tetrahedrons	Fibers	Films	Irregular
Kowalski et al. (2016)	✓	✓								✓
Khatmullina and Isachenko (2017)	✓	✓						✓		
Waldschläger and Schüttrumpf (2019)	✓	✓						✓		✓
Van Melkebeke et al. (2020)								✓	✓	✓
Francalanci et al. (2021)	✓	✓								✓
Wang et al. (2021)	✓									✓
Nguyen (2021)										✓
Khatmullina and Chubarenko (2021)								✓		
Nguyen et al. (2022)								✓		
Yu et al. (2022)	✓	✓						✓		✓
Guler et al. (2022)	✓		✓	✓	✓	✓				
Present	✓	✓	✓	✓	✓	✓	✓	✓		✓

methods, such as Stokes (1851), Camenen (2007), and Zhiyao et al. (2008). Additionally, they proposed new equations to calculate the settling and rise velocities of microplastic particles tailored for specific shapes. Francalanci et al. (2021) measured settling velocities of microplastic particles having shapes corresponding to pellets (characterized as spheres and cylinders in Table 1) and fragments. They analyzed the accuracy of several existing settling velocity equations, such as those of Ferguson and Church (2004), Khatmullina and Isachenko (2017), and Waldschläger and Schüttrumpf (2019). They also proposed a new method to find the settling velocities of microplastic particles having different shapes. Nguyen (2021) conducted experiments with irregular polystyrene microplastic particles to understand their settling behavior and proposed a set of settling velocity equations based on different operational circularity ranges. Khatmullina and Chubarenko (2021) and Nguyen et al. (2022) performed experiments with microplastic fibers, investigating both their settling patterns and velocities. They found high variation in the settling velocity of the fibers due to their different settling orientations. Lastly, Yu et al. (2022) recently conducted a literature review on the settling velocity of microplastic particles and collected an extensive experimental data set from several of the works above (reported between 2016 and 2021). They proposed a new predictive formulation, valid for both regularly- and irregularly-shaped particles. They systematically analyzed the accuracy of their formulation against numerous others from the literature (Song et al., 2008; Alcerreca et al., 2013; Chubarenko et al., 2016; Song et al., 2017; Waldschläger and Schüttrumpf, 2019; Francalanci et al., 2021; Wang et al., 2021). They found that the accuracy of their formulation was significantly better than existing formulas, establishing their method as the most accurate published to date. Several other researchers have studied the effect of biofouling, particle growth, ambient water salinity, and weathering on the settling behavior of microplastic particles (see e.g. Chee et al., 2019; Waldschläger et al., 2020; Nguyen et al., 2020; Brewer et al., 2021; Mendrik et al., 2023). However, the present study will only consider the settling velocity of clean microplastic particles, similar to the studies summarized in Table 1.

As seen in Table 1, several prior experimental works have investigated the settling velocities of microplastic particles having regular shapes such as spheres, cylinders and fibers, as well as irregularly-shaped particles. Other regular shapes such as disks, plates, cubes, other cuboids, and tetrahedrons have not been nearly as extensively studied. (Note that the particles for which settling velocity was reported in the wave flume experiments of Guler et al., 2022, are included in Table 1 for completeness. These have been part of the present experimental campaign and will therefore be treated as a sub-set of those presented in much greater detail herein.) Additionally, most of the available data consider Reynolds numbers in the range $< 10^2$, whereas many microplastic shapes can result in values up to say 10^3. The motivations of the present paper are therefore three-fold: (1) We will present results from novel experiments investigating the settling velocity of microplastic particles having a wider variety of shapes than prior studies, as summarized in Table 1; (2) The experiments will generally span a Reynolds number range 10^2–10^3, thus extending the range covered by much of the existing data; and (3) We will analyze the present data, combined with the extensive data set collected by Yu et al. (2022), on a shape-by-shape basis, leading to yet further increased predictive accuracy for the settling velocity of both regularly- and irregularly-shaped microplastic particles.

The remainder of the present paper is organized as follows: The microplastic particles used in the present experiments, as well as the experimental setup and procedure, are detailed in Section 2. Theoretical considerations and dimensional analysis are reviewed in Section 3. Results are analyzed, and predictive formulations proposed, in Section 4. The accuracy of the present predictive formulations are compared with the method of Yu et al. (2022) in Section 5. Finally, conclusions are drawn in Section 6. Additional applications on predicting the settling velocity of natural sediments are provided in Appendix A.

2. Materials, experimental setup and procedure

2.1. Microplastic particles

Settling velocity experiments were conducted using 66 microplastic particle groups. Photographs of particles representing each group are provided in Fig. 1, with millimetric paper as background, and with the particle number also indicated. The majority (58) of the microplastic particle groups considered have regular shapes, corresponding to: spheres (five), circular cylinders (nine), circular disks (eight), square plates (five), cubes (eight), other cuboids (10 square prisms and six rectangular prisms), tetrahedrons (three), as well as fibers (four). Basic information for each of these regularly-shaped particles are provided in Table 2. This includes the assigned particle number; shape; plastic material; dimensions, where a, b, and c respectively correspond to the longest, intermediate and shortest particle axis (such that $a \geq b \geq c$); nominal diameter (the diameter of a volume-equivalent sphere)

$$d_n = \sqrt[3]{\frac{6\mathcal{V}}{\pi}}, \tag{1}$$

where $\mathcal{V}$ is the particle volume; the Corey (1949) shape factor

$$CSF = \frac{c}{\sqrt{ab}}; \tag{2}$$

sphericity

$$\psi = \frac{A_{s,\text{sphere}}}{A_s}, \tag{3}$$

where $A_{s,\text{sphere}} = 4\pi(d_n/2)^2$ is the surface area of the volume-equivalent sphere, and A_s is the surface area of the particle; and particle density ρ_p. Other quantities appearing in Table 2 will be clearly defined in what follows. Note again that 18 of the particle groups (1–5, 15, 19, 23–25,

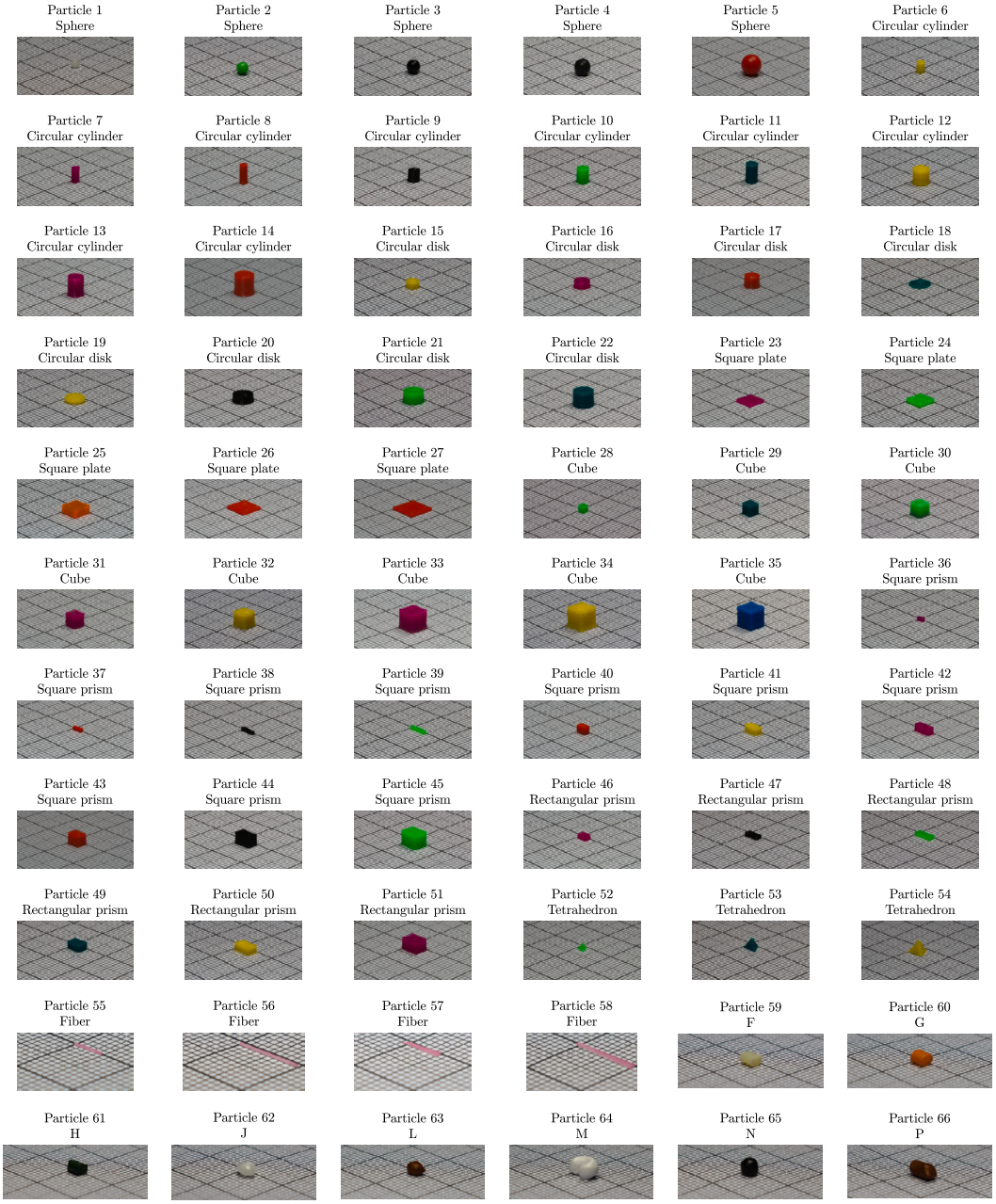

Fig. 1. Photographs of microplastic particles representing each of the 66 groups considered in the present experiments. Particles are lying on millimetric paper.

28, 30, 31, 33–35, 39, and 46) were also used in separate wave flume experiments of Guler et al. (2022), where their settling velocities were also reported. As mentioned above, these will simply be treated as part of the present data set in what follows.

Spheres were purchased from a local supplier. Circular cylinders, circular disks, square plates, cubes, other cuboids, and tetrahedrons were all produced using a 3D printer (Creality Ender-3 V2), with a printing precision of approximately ± 0.1 mm. Fibers were cut from a new dish brush (particle groups 55 and 56) and dental floss (particle groups 57 and 58).

In addition to the regular shapes discussed above, we will likewise newly measure settling velocities for eight irregularly-shaped microplastic particle groups (particle groups 59–66), previously utilized in the wave flume experiments of Kerpen et al. (2020). These specifically correspond to their particle groups F, G, H, J, L, M, N, and P, with their naming convention maintained in the present work. Basic information for each of these particle groups is listed in Table 3, in a similar fashion as in Table 2. Here particle characteristics are taken as reported in Kerpen et al. (2020). Note that the names of plastic materials of these irregularly-shaped microplastic particles are not presented, as they are unknown. These irregularly-shaped particles will likewise be treated as part of the present data set in what follows.

The microplastic particle densities ρ_p for particles having regular shapes have been determined through titration, inspired by the ISO (2012) standard. The procedure followed is as explained in Khatmullina and Isachenko (2017) and Guler et al. (2022).

For later use and summary purposes, each of the shapes to be considered in what follows are indicated in Table 4, along with the definition of several defining or characteristic parameters. When relevant, the diameter d is invoked in these characterizations. Quantities not yet defined, but appearing in Table 4, will again be clearly introduced in what follows.

Table 2
Summary of characteristics and results for the regularly-shaped microplastic particle groups considered in the present experiments. Values a, b, c, d_D, d_n, d_p are defined in Table 4; *CSF* in Eq. (2), ψ in Eq. (3), Re_p in Eq. (14), C_D in Eq. (6); ρ_p is particle density, w_s is settling velocity, and σ_s is the standard deviation of settling velocity.

No.	Shape	Material*	Dimensions (mm)			d_D (mm)	d_n (mm)	d_p (mm)	*CSF*	ψ	ρ_p (kg/m^3)	w_s (m/s)	σ_s (m/s)	Re_p	C_D
			a	b	c										
1	Sphere	POM	2.0	2.0	2.0	2.0	2.0	2.0	1.0	1.0	1353	0.116	0.002	236	0.69
2	Sphere	POM	3.0	3.0	3.0	3.0	3.0	3.0	1.0	1.0	1352	0.161	0.003	491	0.54
3	Sphere	ABS	3.1	3.1	3.1	3.1	3.1	3.1	1.0	1.0	1062	0.059	0.007	185	0.75
4	Sphere	POM	4.0	4.0	4.0	4.0	4.0	4.0	1.0	1.0	1352	0.203	0.002	825	0.45
5	Sphere	POM	5.0	5.0	5.0	5.0	5.0	5.0	1.0	1.0	1358	0.223	0.004	1135	0.47
6	Circular cylinder	PLA	3.0	2.0	2.0	2.4	2.6	2.6	0.82	0.86	1181	0.087	0.002	232	0.74
7	Circular cylinder	PLA	4.0	2.0	2.0	2.4	2.9	2.9	0.71	0.83	1212	0.090	0.002	263	0.82
8	Circular cylinder	PLA	5.0	2.0	2.0	2.4	3.1	3.1	0.63	0.80	1215	0.091	0.003	286	0.82
9	Circular cylinder	PLA	3.0	3.0	3.0	3.5	3.4	3.4	1.0	0.87	1218	0.101	0.005	352	1.00
10	Circular cylinder	PLA	4.0	3.0	3.0	3.5	3.8	3.8	0.87	0.87	1196	0.107	0.005	410	0.80
11	Circular cylinder	PLA	5.0	3.0	3.0	3.5	4.1	4.1	0.77	0.85	1192	0.111	0.006	458	0.73
12	Circular cylinder	PLA	4.0	4.0	4.0	4.7	4.6	4.6	1.0	0.87	1191	0.109	0.007	507	1.00
13	Circular cylinder	PLA	5.0	4.0	4.0	4.7	4.9	4.9	0.89	0.87	1195	0.121	0.007	604	0.84
14	Circular cylinder	PLA	5.0	5.0	5.0	5.9	5.7	5.7	1.0	0.87	1194	0.125	0.010	728	0.97
15	Circular disk	PLA	3.0	3.0	2.0	3.0	3.0	3.0	0.67	0.86	1195	0.086	0.010	263	1.04
16	Circular disk	PLA	4.0	4.0	2.0	3.0	3.6	4.0	0.50	0.83	1207	0.089	0.004	364	1.03
17	Circular disk	PLA	4.0	4.0	3.0	4.5	4.2	4.0	0.75	0.87	1185	0.100	0.005	407	1.10
18	Circular disk	PLA	5.0	5.0	0.5	0.8	2.7	5.0	0.10	0.47	1213	0.045	0.002	226	1.06
19	Circular disk	PLA	5.0	5.0	1.0	1.5	3.3	5.0	0.20	0.64	1193	0.056	0.002	286	1.21
20	Circular disk	PLA	5.0	5.0	2.0	3.0	4.2	5.0	0.40	0.79	1215	0.082	0.007	419	1.25
21	Circular disk	PLA	5.0	5.0	3.0	4.5	4.8	5.0	0.60	0.85	1205	0.107	0.007	545	1.06
22	Circular disk	PLA	5.0	5.0	4.0	6.0	5.3	5.0	0.80	0.87	1208	0.118	0.005	599	1.19
23	Square plate	PLA	5.0	5.0	0.5	0.8	2.9	5.0	0.10	0.43	1206	0.041	0.001	210	1.20
24	Square plate	PLA	5.0	5.0	1.0	1.5	3.6	5.0	0.20	0.59	1197	0.057	0.001	289	1.21
25	Square plate	PLA	5.0	5.0	2.0	3.0	4.6	5.0	0.40	0.73	1202	0.081	0.004	410	1.23
26	Square plate	PLA	6.0	6.0	0.5	0.8	3.3	6.0	0.08	0.40	1217	0.042	0.002	258	1.20
27	Square plate	PLA	7.0	7.0	0.5	0.8	3.6	7.0	0.07	0.36	1213	0.041	0.003	289	1.28
28	Cube	PLA	2.0	2.0	2.0	3.0	2.5	2.0	1.0	0.81	1195	0.091	0.005	185	0.93
29	Cube	PLA	3.0	3.0	3.0	4.5	3.7	3.0	1.0	0.81	1199	0.098	0.005	299	1.23
30	Cube	PLA	3.5	3.5	3.5	5.3	4.3	3.5	1.0	0.81	1187	0.105	0.006	372	1.19
31	Cube	PLA	3.5	3.5	3.5	5.3	4.3	3.5	1.0	0.81	1143	0.096	0.006	340	1.09
32	Cube	PLA	4.0	4.0	4.0	6.0	5.0	4.0	1.0	0.81	1192	0.105	0.005	427	1.38
33	Cube	PLA	5.0	5.0	5.0	7.5	6.2	5.0	1.0	0.81	1184	0.124	0.004	629	1.19
34	Cube	PLA	5.0	5.0	5.0	7.5	6.2	5.0	1.0	0.81	1100	0.100	0.009	509	1.00
35	Cube	PLA	5.0	5.0	5.0	7.5	6.2	5.0	1.0	0.81	1076	0.089	0.007	453	0.97
36	Square prism	PLA	2.0	1.0	1.0	1.5	1.6	1.4	0.71	0.77	1199	0.051	0.004	73	1.52
37	Square prism	PLA	3.0	1.0	1.0	1.5	1.8	1.7	0.58	0.72	1212	0.056	0.001	98	1.35
38	Square prism	PLA	4.0	1.0	1.0	1.5	2.0	2.0	0.50	0.68	1218	0.054	0.003	109	1.49
39	Square prism	PLA	5.0	1.0	1.0	1.5	2.1	2.2	0.45	0.64	1208	0.052	0.004	118	1.53
40	Square prism	PLA	3.0	2.0	2.0	3.0	2.8	2.4	0.82	0.79	1197	0.083	0.005	208	1.12
41	Square prism	PLA	4.0	2.0	2.0	3.0	3.1	2.8	0.71	0.77	1205	0.086	0.009	248	1.09
42	Square prism	PLA	5.0	2.0	2.0	3.0	3.4	3.2	0.63	0.74	1208	0.083	0.002	265	1.21
43	Square prism	PLA	4.0	3.0	3.0	4.5	4.1	3.5	0.87	0.80	1188	0.094	0.005	331	1.27
44	Square prism	PLA	5.0	3.0	3.0	4.5	4.4	3.9	0.77	0.78	1206	0.096	0.006	378	1.33
45	Square prism	PLA	5.0	4.0	4.0	6.0	5.3	4.5	0.89	0.80	1205	0.110	0.005	498	1.35
46	Rectangle prism	PLA	3.0	2.0	1.0	1.5	2.3	2.4	0.41	0.73	1202	0.055	0.002	138	1.31
47	Rectangle prism	PLA	4.0	2.0	1.0	1.5	2.5	2.8	0.35	0.69	1211	0.056	0.005	160	1.34
48	Rectangle prism	PLA	5.0	2.0	1.0	1.5	2.7	3.2	0.32	0.66	1215	0.054	0.003	174	1.45
49	Rectangle prism	PLA	4.0	3.0	2.0	3.0	3.6	3.5	0.58	0.77	1205	0.083	0.005	292	1.19
50	Rectangle prism	PLA	5.0	3.0	2.0	3.0	3.9	3.9	0.52	0.75	1205	0.081	0.009	319	1.24
51	Rectangle prism	PLA	5.0	4.0	3.0	4.5	4.9	4.5	0.67	0.79	1202	0.100	0.003	455	1.20
52	Tetrahedron	PLA	3.0	2.6	2.4	1.2	1.8	3.0	0.88	0.67	1195	0.054	0.004	163	1.10
53	Tetrahedron	PLA	4.0	3.5	3.3	1.6	2.4	4.0	0.88	0.67	1184	0.058	0.005	235	1.19
54	Tetrahedron	PLA	5.0	4.3	4.1	2.0	3.0	5.0	0.88	0.67	1180	0.066	0.004	335	1.12
55	Fiber	Nylon	5.0	0.35	0.35	0.4	1.0	1.0	0.26	0.52	1146	0.017	0.001	16	2.89
56	Fiber	Nylon	10.0	0.35	0.35	0.4	1.2	1.2	0.19	0.42	1146	0.017	0.001	21	2.78
57	Fiber	Nylon	5.0	0.8	0.1	0.1	0.8	0.8	0.05	0.14	1134	0.011	0.001	9	1.85
58	Fiber	Nylon	10.0	0.8	0.1	0.1	1.1	1.1	0.04	0.11	1134	0.011	0.001	12	1.79

* PLA: Polylactic Acid, POM: Polyoxymethylene, ABS: Acrylonitrile Butadiene Styrene.

2.2. Experimental setup and procedure

Settling velocity experiments were conducted in a clear graduated cylinder having diameter 6.9 cm and height 53.5 cm. The container was filled with distilled water and placed in front of a vertical plate, which was covered with a 2×2 cm checkerboard pattern to support determination of the particle position. The distilled water temperature was measured daily with a digital thermometer and was found to be nearly constant with a mean of 20.8 °C and standard deviation of 0.5 °C, where the density and kinematic viscosity of water correspond to $\rho = 998$ kg/m^3 and $\nu = 0.984 \times 10^{-6}$ m^2/s, respectively. A light source was placed on top of the container to increase the visibility of the microplastic particles as they settled. A Nikon D5600 camera was used to record the settling of the microplastic particles in Full HD resolution (1920×1080 pixels) at 60 frames per s. The camera was focused on a section spanning from ≈ 0.1 m below the water surface to ≈ 0.1 m above the container bottom, to enable detailed tracking of the particles. Camera calibration was performed in situ, using a ruler in the center of the filled container prior to the experiments. The graduation on the cylinder and the back plate with checkerboard pattern confirmed the initial

Table 3
Summary of characteristics and results for the irregularly-shaped microplastic particle groups considered in the present experiments, from Kerpen et al. (2020). Values a, b, c, d_D, d_n, d_p are defined in Table 4; *CSF* in Eq. (2), ψ in Eq. (3), Re_p in Eq. (14), C_D in Eq. (6); ρ_p is particle density, w_s is settling velocity, and σ_s is the standard deviation of settling velocity.

No.	Particle code	Dimensions* (mm)			d_D (mm)	d_n (mm)	d_p (mm)	*CSF*	ψ	ρ_p (kg/m^3)	w_s (m/s)	σ_s (m/s)	Re_p	C_D
		a	b	c										
59	F	3.37	3.05	2.48	2.48	2.94	3.21	0.77	0.84	1027	0.036	0.003	118	0.71
60	G	3.19	2.94	2.35	2.35	2.80	3.06	0.77	0.84	1051	0.041	0.004	126	0.99
61	H	2.98	2.40	2.37	2.37	2.57	2.67	0.89	0.92	1198	0.113	0.018	306	0.49
62	J	3.89	3.06	2.16	2.16	2.95	3.45	0.63	0.73	1343	0.115	0.006	403	0.74
63	L	3.59	2.77	2.62	2.62	2.96	3.15	0.83	0.88	1637	0.180	0.010	576	0.68
64	M	4.78	3.37	2.93	2.93	3.61	4.01	0.73	0.81	1263	0.115	0.022	469	0.77
65	N	3.82	3.47	3.21	3.21	3.49	3.64	0.88	0.92	1133	0.098	0.007	364	0.59
66	P	5.02	3.98	2.86	2.86	3.85	4.47	0.64	0.74	1983	0.204	0.020	929	0.88

* Dimensions, ψ, and ρ_p values are given based on Kerpen et al. (2020).

Table 4
Summary of characteristic lengths and other parameters for each shape considered in the present work. The final two columns respectively provide the recommended predictive drag coefficient C_D, defined in Eq. (6), as well as the applicable range of Reynolds number Re_p, defined in Eq. (14).

Sphere	Circular cylinder	Elliptical cylinder	Circular disk	Square plate	Cube	Square prism	Rectangular prism	Tetrahedron
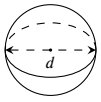	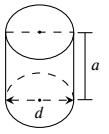	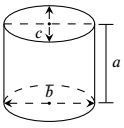	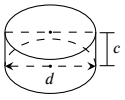	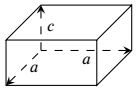	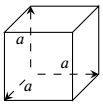	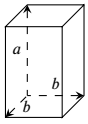	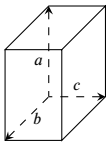	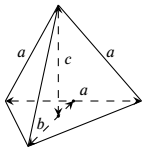

Shape	Dimensions			$\mathcal{V}$	A	d_D	d_n	d_p	C_D	Re_p
	a	b	c							
Sphere	d	d	d	$\frac{\pi}{6}d^3$	$\frac{\pi}{4}d^2$	d	d	d	Eq. (17)	
Circular cylinder	a	d	d	$\frac{\pi}{4}d^2a$	ad	$\frac{3\pi d}{8}$	$\sqrt[3]{\frac{3}{2}d^2a}$	d_n	Eq. (19)	≥ 1
Elliptical cylinder	a	b	c	$\frac{\pi}{4}abc$	ab	$\frac{3\pi c}{8}$	$\sqrt[3]{\frac{3}{2}abc}$	d_n	Eq. (19)	> 10
Circular disk	d	d	c	$\frac{\pi}{4}d^2c$	$\frac{\pi}{4}d^2$	$\frac{3c}{2}$	$\sqrt[3]{\frac{3}{2}d^2c}$	d	1.12	> 220
Square plate	a	a	c	a^2c	a^2	$\frac{3c}{2}$	$\sqrt[3]{\frac{6}{\pi}a^2c}$	a	1.23	> 200
Cube	a	a	a	a^3	a^2	$\frac{3a}{2}$	$\sqrt[3]{\frac{6}{\pi}a}$	a	1.12	> 180
Square prism	a	b	b	ab^2	ab	$\frac{3b}{2}$	$\sqrt[3]{\frac{6}{\pi}ab^2}$	$\sqrt{ab}$	1.31	> 70
Rectangular prism	a	b	c	abc	ab	$\frac{3c}{2}$	$\sqrt[3]{\frac{6}{\pi}abc}$	$\sqrt{ab}$	1.31	> 70
Tetrahedron	a	$\frac{\sqrt{3}}{2}a$	$\sqrt{\frac{2}{3}}a$	$\frac{\sqrt{2}}{12}a^3$	$\frac{\sqrt{3}}{4}a^2$	$\frac{a}{\sqrt{6}}$	$\sqrt[3]{\frac{1}{\pi\sqrt{2}}a}$	a	1.14	> 160
Fiber	(Modeled as circular or elliptical cylinder.)								Eq. (19)	> 1
Irregular	a	b	c	$\frac{\pi}{6}abc$	$\frac{\pi}{4}ab$	c	$\sqrt[3]{abc}$	$\sqrt{ab}$	Eq. (20)	> 0.4

calibration during the experiments. Each particle was released from a distance of 1 cm below the water surface to break surface tension and eliminate potential bubble formation on the surface of the particle. For each particle group, tests were repeated until the settling of 20 individual particles were recorded. Recordings were accepted if particles settled close to the centerline of the cylinder container, avoiding any contact with the side.

The video recordings of the microplastic particles were analyzed using an image processing algorithm based on color tracking, similar to that described by Goral et al. (2021). To determine the terminal settling velocity w_s, the duration after which particles have effectively reached their terminal settling velocities were identified. This duration is assumed to begin at the time where the change in $w_s(t)$ determined from the time derivative of the vertical particle position, between two successive time intervals first varied less than 1%. The duration considered for analysis then ends at the time where settling particles started to exit the recording section, where false tracking of particles began, due to the reduced color-tracked area. The various $w_s(t)$ signals were then individually averaged over these temporal durations. Reported values for the terminal settling velocity w_s correspond to the mean of those obtained from the 20 individual repetitions. These values, as well as the corresponding standard deviations σ_s (computed from the same sample), are reported in Tables 2 and 3.

3. Theoretical considerations and dimensional analysis

3.1. Theoretical considerations

Let us now review, from first principles, the basic mechanics of a foreign particle settling in a fluid at its terminal settling velocity. At terminal velocity, the combined gravitational and buoyancy forces (submerged weight)

$$W = g\left(\rho_p - \rho\right)\mathcal{V} \tag{4}$$

will be in balance with the drag force

$$F_D = \frac{1}{2}C_D\rho w_s^2 A \tag{5}$$

which is formulated in the standard way in terms of a drag coefficient C_D. Equating these, and re-arranging, then leads to the following definition of the drag coefficient

$$C_D = \frac{2g\,(s-1)\,\mathcal{V}}{w_s^2 A} = \frac{4g(s-1)d_D}{3w_s^2}, \tag{6}$$

where $s = \rho_p/\rho$ is the relative density of the particle. In the above

$$d_D = \frac{3\mathcal{V}}{2A} \tag{7}$$

is the implied length scale required to achieve a drag coefficient having the same form as for spheres when written in term of their diameter d (see Eq. (8) just below). We emphasize that the above is generically formulated in terms of the particle's volume $\mathcal{V}$ and projected area A. No particular particle shape or orientation is yet assumed.

Now, in the special case where the particle is a sphere, $A = \pi d^2/4$, $\mathcal{V} = \pi d^3/6$ and $d_D = d$, such that Eq. (6) simplifies to

$$C_{D,\,\text{sphere}} = \frac{4g(s-1)d}{3w_s^2}. \tag{8}$$

Presumably based on this, several researchers investigating the settling velocity of microplastic particles (e.g. Waldschläger and Schüttrumpf, 2019; Francalanci et al., 2021; Wang et al., 2021; Yu et al., 2022) have utilized a drag coefficient effectively defined in terms of the nominal diameter

$$C_n = \frac{4g(s-1)d_n}{3w_s^2} \tag{9}$$

(or something directly proportional to d_n), rather than strictly as formulated in Eq. (6). This is an important distinction, since C_n is at best only generally an approximation of C_D. It fundamentally assumes that $d_D \sim d_n$ (equivalently that $A \sim d_n^2$, as explicitly formulated by Francalanci et al., 2021, see their Eq. 4). Since $d_n \sim (abc)^{1/3}$, i.e. it depends on all three particle dimensions (raised to the same power), this assumes that settling particles will have no preferential orientation. Our own experimental observations have indicated that this assumption is generally incorrect, however, especially for particles having large differences in their fundamental dimensions a, b and c (flat or elongated particles e.g. cylinders, disks and thin plates).

Based on our experimental observations (see also the prior observations and discussion of Guler et al., 2022), microplastic particles tend to settle with their broadest face (largest projected area) normal to the predominant line of motion. Similar observations have, in fact, long been made for natural sediments dating back at least to Rubey (1933) and Wadell (1935), as noted by Corey (1949). This observation was likewise the stated inspiration of Corey (1949) in the formulation of his shape factor *CSF*, Eq. (2), intended as a measure of flatness. To exemplify the fundamental importance of this preferential orientation, compare the tabulated d_D values in Table 4 for a variety of shapes with their respective d_n, where $\mathcal{V}$ and A are as specified there. Regardless of shape, since $d_D \sim \mathcal{V}/A$, it is always directly proportional to the shortest of the particles' three dimensions, c (i.e. the numerator in *CSF*). This is obviously fundamentally different than d_n, which again weighs all three dimensions (a, b and c) with equal power. It is, in fact, trivial to show that

$$d_D \sim d_n \cdot CSF^{2/3}, \tag{10}$$

and therefore that

$$C_D \sim C_n \cdot CSF^{2/3}, \tag{11}$$

such that length scales d_D and d_n (hence C_D and C_n) can only be properly interchanged in special cases where $CSF = 1$ (e.g. spheres and cubes).

As a consequence, especially for flat or elongated particles (e.g. cylinders and flat disks or plates), formulations based on a "drag coefficient" defined as C_n in Eq. (9), rather than as in Eq. (6), will neglect any preferential settling orientation. This, in turn, may introduce unnecessary scatter and/or false Reynolds number dependence in experimental data. Some selected examples demonstrating precisely these phenomena will be directly shown in what follows. Note that maintaining a clearly defined characteristic projection area A, likewise has the added benefit that results for a given particle shape can be reconciled with (or at least compared to) drag coefficient results for fixed regular shapes as e.g. commonly found in many basic fluid mechanics textbooks.

Of all the recently published papers specifically on the settling velocity of microplastic particles (e.g. Kowalski et al., 2016; Khatmullina and Isachenko, 2017; Waldschläger and Schüttrumpf, 2019; Van Melkebeke et al., 2020; Francalanci et al., 2021; Wang et al., 2021; Yu et al., 2022), it seems that none have attempted to uniformly maintain a drag coefficient consistent with Eq. (6) in their final formulations. Notably, Khatmullina and Isachenko (2017) defined C_D appropriately in their Eq. 1, as well as A appropriately (for cylinders) leading to their Eq. 9, but did not maintain a dimensionally-consistent parameterization leading up to their final settling velocity formula (their Eq. 13). Waldschläger and Schüttrumpf (2019) have seemingly defined C_D appropriately for fibers, utilizing $d_D = c$ in their Eq. 8, but utilized $d_D \sim d_n$ for other non-spherical shapes (pellets and fragments). Others (Kowalski et al., 2016) either did not utilize a drag coefficient in their parameterizations, or did not clearly define it (Van Melkebeke et al., 2020). A parameterization making clear and strict use of C_D, as defined in Eq. (6), while properly accounting for observed preferential particle settling orientation, will be uniformly sought in the present work.

3.2. Dimensional analysis

In addition to the theoretical considerations above, for the sake of completeness, we will now review the traditional formulation of the settling velocity problem on purely dimensional grounds. The determining drag force on a settling particle will depend on the following physical parameters

$$F_D = f\left(\rho,\, \nu,\, d_p,\, w_s,\, \text{shape}\right), \tag{12}$$

where d_p is a characteristic particle length scale, 'shape' refers to the microplastic particle shape (see Table 4 and Fig. 1), and $f(\cdot)$ refers to some (as yet, unknown) function. Standard dimensional analysis then leads to the classical expectation that

$$C_D = f\left(Re_p,\, \text{shape}\right), \tag{13}$$

where

$$Re_p = \frac{w_s d_p}{\nu} \tag{14}$$

is the Reynolds number. Note that, unlike the length scale d_D in the drag coefficient, the characteristic length scale in the Reynolds number d_p may be conveniently chosen for each particle shape, e.g. either on physical grounds (such that $d_p^2 \sim A$) or to achieve the best clustering of experimental data. In what follows, we will make strict use of the d_p values as defined for each shape in Table 4.

For later use, the Reynolds number specifically utilizing d_n as the length scale is defined as

$$Re_n = \frac{w_s d_n}{\nu}. \tag{15}$$

Obviously, in special cases where $d_p = d_n$, these two Reynolds numbers are equivalent, but we emphasize that this is not generally valid in the present work.

4. Results

Based on both the theoretical considerations and dimensional analysis considered in the preceding section, we will now present and analyze the results of the present experimental data set, which again includes a variety of microplastic particle shapes. To begin, the present experimental results are summarized in Fig. 2 in the classical fashion (drag coefficient C_D versus Reynolds number Re_p), with characteristic variables again strictly as defined in Table 4. Also plotted as lines on Fig. 2, for reference and preliminary comparison, are the theoretical Stokes (1851) law

$$C_D = \frac{24}{Re_p} \tag{16}$$

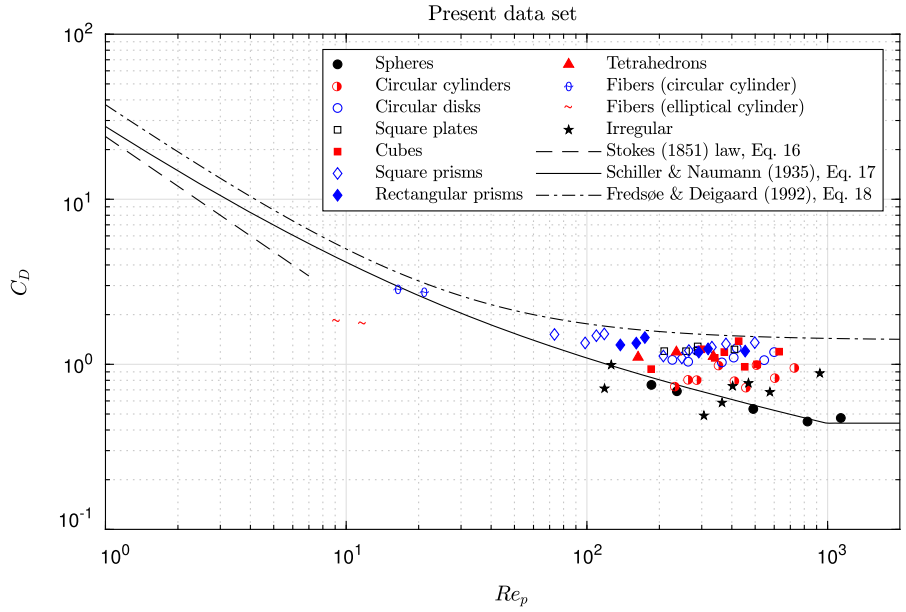

Fig. 2. Summary of measured drag coefficients C_D versus Reynolds number Re_p for all settling microplastic particles tested in the present experiments.

for predicting the drag coefficient (hence settling velocity) of spheres for low $Re_p \ll 1$, the empirical drag coefficient for spheres of Schiller and Naumann (1935)

$$C_D = \max\left[\frac{24}{Re_p}\left(1 + 0.15Re_p^{0.687}\right), 0.44\right], \tag{17}$$

as well as the empirical drag coefficient formulation of Fredsøe and Deigaard (1992)

$$C_D = 1.4 + \frac{36}{Re_p}, \tag{18}$$

designed for predicting the settling velocity of natural sediments. The latter is included as reference here because it was used to estimate microplastic settling velocities by Alsina et al. (2020). It is seen that most of the C_D values from the present data set lie between the formulation of Schiller and Naumann (1935) and that of Fredsøe and Deigaard (1992). Most of the present data lies in the range $10^2 \leq Re_p \leq 10^3$, whereas that from most existing studies on settling velocity of microplastics have primarily considered smaller particles with $Re \leq 10^2$.

In addition, we will likewise consider and collectively analyze the extensive data set for microplastic settling velocities recently compiled and made digitally available by Yu et al. (2022). This data includes those from the following prior studies: Kowalski et al. (2016), Khatmullina and Isachenko (2017), and Van Melkebeke et al. (2020), as explained in detail therein. Data from Waldschläger and Schüttrumpf (2019), Wang et al. (2021) and Francalanci et al. (2021) were filtered out by Yu et al. (2022), due to a lack of sufficient information available for calculation of shape descriptors (*CSF* and ψ). In line with expectations based on Eq. (13), results will be considered in terms of the drag coefficient defined in Eq. (6), and will henceforth be analyzed on a shape-by-shape basis.

4.1. Spheres

Let us first analyze results for microplastic spheres. For this purpose, we will consider the present results from Table 2, as well as the additional data for spheres compiled by Yu et al. (2022). For spheres the characteristic projection area is obviously that of a circle $A = \pi d^2/4$ and their characteristic length scale is naturally taken as their diameter $d_p = d$.

All available results for spherical microplastic particles are plotted in the classical fashion (again, drag coefficient C_D versus Reynolds number Re_p) in Fig. 3. It is seen that the spherical microplastic particles compiled by Yu et al. (2022) primarily span $Re < 10^2$, whereas those from the present study again span $Re > 10^2$. All of the sphere data cluster tightly and convincingly around the empirical formulation of Schiller and Naumann (1935), Eq. (17), presented as the full line. This formulation hence seems excellently suited for predicting the settling velocity of microplastic spheres, and is therefore recommended.

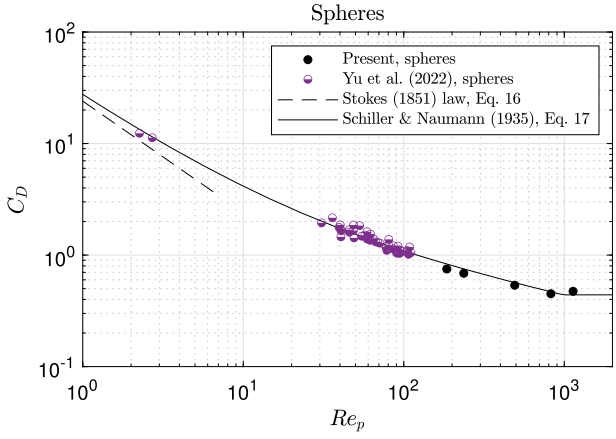

Fig. 3. Measured drag coefficients C_D versus Reynolds number Re_p for settling microplastic spheres.

4.2. Cylinders and fibers

Let us now consider the settling velocity of microplastic cylinders. Due to their reasonable similarity in shape, we will collectively combine these data with those for fibers in this sub-section. For this purpose, we will again consider relevant results from the present data set, which includes the 3D printed cylinders (particle groups 6–14). Additionally, we will likewise respectively analyze the present data for dish brush fibers (particle groups 55 and 56) and dental floss fibers (particle groups 57 and 58) as circular and elliptical cylinders, respectively. These will be combined with the data for fibers compiled by Yu et al. (2022), comprised of both fishing line segments (assumed circular in cross section, since $b = c$), as well as other cylinders where $b \neq c$ (assumed elliptical

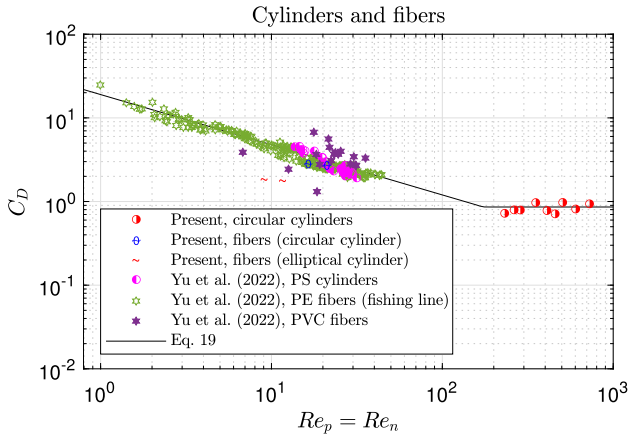

Fig. 4. Measured drag coefficients C_D versus Reynolds number Re_p for settling cylindrical microplastic particles, including fibers.

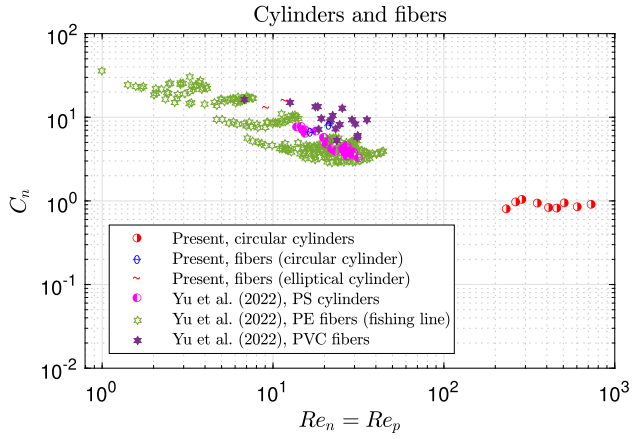

Fig. 5. Measured C_n values versus Reynolds number Re_n for settling cylindrical microplastic particles, including fibers. Note the increased scatter relative to Fig. 4.

in cross section). Unless otherwise stated, all characteristic parameters are again strictly as defined in Table 4.

Based on our experimental observations, in line with our discussion in Section 3.1, cylinders tend to settle with their long axis predominantly horizontal, such that the characteristic projection area may be reasonably approximated as $A = ab$. In defining the length scale to be utilized in the Reynolds number Re_p, the best (tightest) clustering of the data has been achieved, in this case, simply by taking $d_p = d_n$. For the present cylinders and fibers, d_n is calculated as in Table 4, whereas we utilize the d_n values explicitly reported by Yu et al. (2022) for the sake of consistency with their work.

Results for combined cylinders and fibers are presented in the classical fashion in Fig. 4. It is seen that, when presented in this fashion, the data cluster convincingly. They are well approximated by the empirical expression

$$C_D = \max\left(19Re_p^{-0.6}, 0.86\right) \tag{19}$$

depicted as the solid line. It can also be seen that the present elliptical fibers do not cluster as convincingly as the other fibers. The reason for this may be due to differences in their flexibility (particle groups 57–58 are far more flexible than particle groups 55–56, see e.g. Khatmullina and Chubarenko, 2021; Nguyen et al., 2022, for further discussions on settling behavior of fibers).

The discussion in Section 3.1 has emphasized the potential importance of using a drag coefficient C_D as defined in Eq. (6), rather than the approximation C_n in Eq. (9), especially for elongated particles. Our

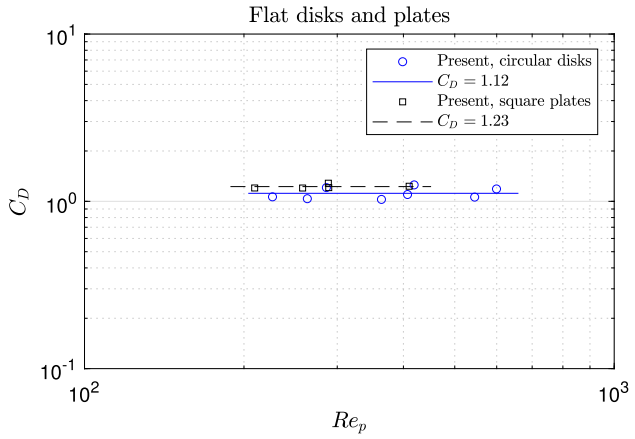

Fig. 6. Measured drag coefficients C_D versus Reynolds number Re_p for settling microplastic circular disks and square plates.

contention that use of C_n may increase scatter is directly tested in Fig. 5, which plots the same data as in Fig. 4, but with C_D on the ordinate replaced by C_n. In line with our contention, comparing Fig. 5 with Fig. 4, it is seen that utilizing C_n introduces considerably more scatter in the data. This supports our contention that, if the preferred settling orientation can be reasonably approximated, the drag coefficient is best defined as in Eq. (6). This is again consistent with theoretical considerations, taking into account that these particles have a preferential settling orientation.

4.3. Flat disks and square plates

Let us now turn our attention to flat circular disks and square plates, which are newly part of the present experimental data set. These two shapes are grouped due to obvious physical similarities in their expected settling hydrodynamics. As described above, our experimental observations have shown that these particles likewise have a preferential settling orientation, i.e. they tend to settle with their largest projection area normal to the predominant line of motion. This is not a unique finding of this study and has also been demonstrated for settling disks elsewhere (see e.g. Willmarth et al., 1964). As such, for circular disks the characteristic length scale is naturally taken as $d_p = d$, with the characteristic projection area taken as the circular face $A = \pi d^2/4$, see Table 4. Analogously, for thin square plates we utilize $d_p = a$ and $A = a^2$. In both cases it is again emphasized that this leads to the length scale within the drag coefficient $d_D = 3c/2$ i.e. proportional to c, and not d_n.

The drag coefficients C_D are plotted versus their respective Reynolds numbers Re_p in the classical fashion in Fig. 6. Both sets of data clearly support constant C_D values over the range of Reynolds number considered ($Re_p > 2 \times 10^2$). Note that the constant (mean value) $C_D = 1.12$ found for the settling disks is very close to that for fixed disks at sufficiently large Reynolds number, see e.g. Figure 16.6 of Petersen (2006). The constant $C_D = 1.23$ presently found for square plates is likewise very close to the value 1.18 suggested for fixed square plates by Roberson and Crowe (1993) for Reynolds numbers $> 10^4$, see their Table 11.1.

We will utilize the present disk and square plate data to further test our contention that the drag coefficient ought to be strictly defined as C_D in Eq. (6), rather than C_n in Eq. (9), now for flat particles. For this purpose, the data from Fig. 6 are re-plotted in Fig. 7, but now using the prevailing fashion i.e. as C_n versus Re_n, as in Fig. 5 above. It is seen from Fig. 7 that adopting this convention based on the use of the nominal diameter d_n as a universal length scale introduces both false Reynolds number dependence, as well as increased scatter, relative to Fig. 6. Note that Reynolds number dependence for settling disks or plates is contrary to their fluid mechanics, since (at sufficiently high Reynolds number) the flow separation points are more or less fixed at their edges, which means that nearly constant drag coefficients can be expected.

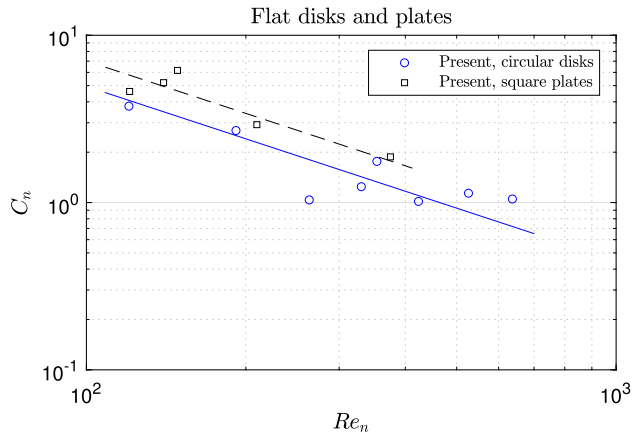

Fig. 7. Measured C_n values versus Reynolds number Re_n for settling microplastic circular disks and plates. Note both the false Reynolds number dependence and increased scatter, relative to Fig. 6.

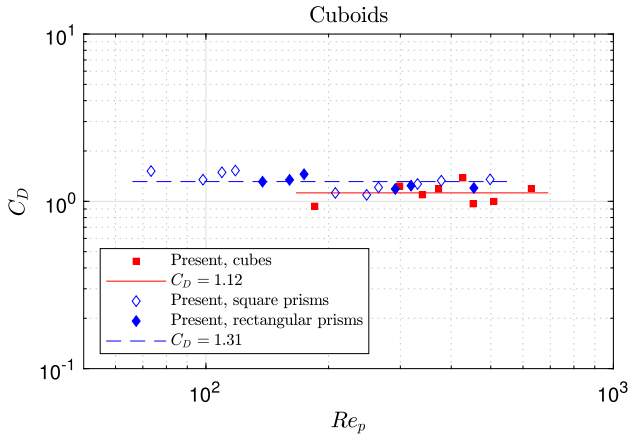

Fig. 8. Measured drag coefficients C_D versus Reynolds number Re_p for settling microplastic cuboids (cubes, square and rectangular prisms).

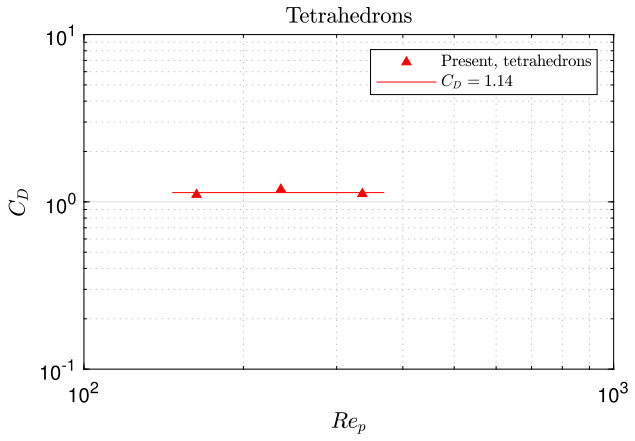

Fig. 9. Measured drag coefficients C_D versus Reynolds number Re_p for settling microplastic tetrahedrons.

This is our second convincing demonstration of unnecessary complexity introduced by the use of C_n (again, seemingly the prevailing convention), rather than C_D. Having established this, for all additional shapes that follow, we will exclusively use C_D in forthcoming analysis of other particle shapes.

4.4. Other cuboids (cubes and rectangular prisms)

We will now consider the settling velocity of more general microplastic cuboids (rectangular prisms, including both cubes and square prisms as special cases), again newly part of the present experimental data set. Based on our experimental observations, and in line with the theoretical discussion above, we take the characteristic projection area as the product of the two largest side lengths $A = ab$. For fundamental consistency with our treatment of square plates (also a cuboid), we adopt the characteristic length scale $d_p = \sqrt{ab}$ for use in the Reynolds number Re_p, see again Table 4. Indeed, it is emphasized that any other choice of A or d_p would present logical inconsistency with our successful parameterization of square plates above.

Notice that the convention arrived at just above leads to a length scale $d_D = c$ within the drag coefficient C_D, again corresponding to the numerator of the Corey (1949) shape factor *CSF*, defined in Eq. (2). Conversely, the parameterization described above leads to a length scale in the Reynolds number (again, $d_p = \sqrt{ab}$) equivalent to the denominator in *CSF*. This is not coincidental. Both the present parameterization, as well as Corey's formulation of *CSF*, were inspired by the observational knowledge that particles tend to settle with their largest projected area normal to the predominant line of motion. While noting these similarities, it is emphasized that we do not utilize *CSF* directly in any of our formulations, as the physics on which it is based are naturally accounted for through our choice of parameterization.

The resulting drag coefficients for cuboids are presented in the classical fashion in Fig. 8. Over the range of Reynolds number considered ($Re_p > 10^2$), the results for settling cubes suggest a simple constant drag coefficient of $C_D = 1.12$. This is again very much in line with the value of 1.1 for flow around fixed cubes at sufficiently high Reynolds number ($> 10^4$), as suggested by Roberson and Crowe (1993), see again their Table 11.1. The present data for the drag coefficients for more general cuboids (square and rectangular prisms) also cluster around a constant, slightly larger, value $C_D = 1.31$. This slightly larger value (relative to cubes) for particles having increased irregularity is also in line with physical expectations.

4.5. Tetrahedrons

We will now analyze the present data for settling microplastic tetrahedron particles. For these we utilize a characteristic projection area corresponding to one of their triangular faces $A = \sqrt{3}a^2/4$, with characteristic length equal to their edge length $d_p = a$. The experimentally obtained drag coefficients are presented in the classical fashion in Fig. 9. The data again suggests that the drag coefficient is effectively constant over the range tested ($Re_p > 10^2$), in this case with mean value of $C_D = 1.14$.

4.6. Irregularly-shaped particles

We will finally consider the settling velocity of irregularly-shaped microplastic particles. The data to be analyzed in what follows includes those for the angular, nodular, and fragmented particles compiled by Yu et al. (2022). It likewise includes the present irregular (though generally less angular) particles listed in Table 3.

In analyzing the settling velocity data of these irregular shaped microplastics, we approximate their volumes as ellipsoids $\mathcal{V} = \pi abc/6$. We have found that the best clustering is achieved by taking the characteristic projection area based on the two longest axes $A = \pi ab/4$, coupled with the length scale $d_p = \sqrt{ab}$. Similar to many of the particle shapes analyzed above, these choices lead to $d_D = c$, such that the drag coefficient again takes into account the shortest particle dimension, with the longest two dimensions (a and b) accounted for in the Reynolds number Re_p, see again Table 4. These choices are once again very much in

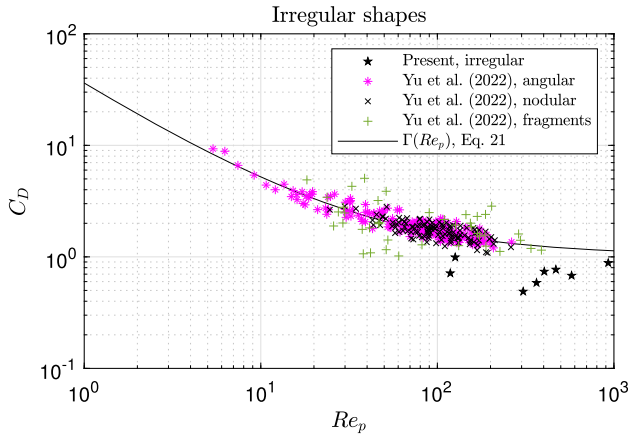

Fig. 10. Measured drag coefficients C_D versus Reynolds number Re_p for settling irregularly-shaped microplastic particles.

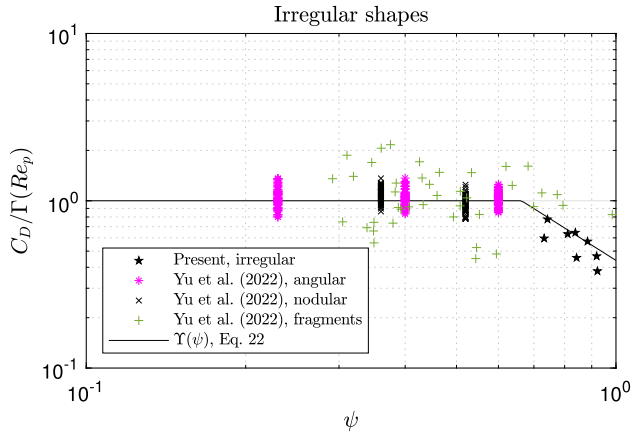

Fig. 11. Measured drag coefficients C_D, normalized by the function $\Gamma(Re_p)$, versus sphericity ψ for settling irregularly-shaped microplastic particles.

line with our general observation, that particles tend to settle with their largest projection area normal to the predominant line of motion.

The drag coefficients for settling irregularly-shaped microplastic particles are plotted in the classical fashion in Fig. 10. Despite the inherent difficulty in uniformly characterizing the wide variety of irregularly-shaped particles being considered, it is seen that the method of parameterization adopted herein still leads to a rather convincing clustering of the data. Most of the scatter is seen to stem from a portion of the fragmented particles. The present irregular particle data (generally having larger sphericity ψ) is also systematically below the rest.

To formulate a predictive model for the settling velocity of irregularly-shaped microplastic particles, let us suppose that the drag coefficient may be formulated as follows

$$C_D = \Gamma(Re_p) \cdot \Upsilon(\psi) \tag{20}$$

where $\Gamma(Re_p)$ and $\Upsilon(\psi)$ are, as yet, unknown functions. This formulation thus conceptually accounts for both primary dependence on the Reynolds number Re_p, and also potential secondary dependence on sphericity ψ, since irregularly-shaped particles are not uniquely defined solely by their three length scales a, b, and c. The primary dependence on Re_p is already evident from Fig. 10. The data are well represented there by the function

$$\Gamma(Re_p) = 1 + \frac{3.2}{\sqrt{Re_p}} + \frac{32}{Re_p} \tag{21}$$

which is depicted as the full line.

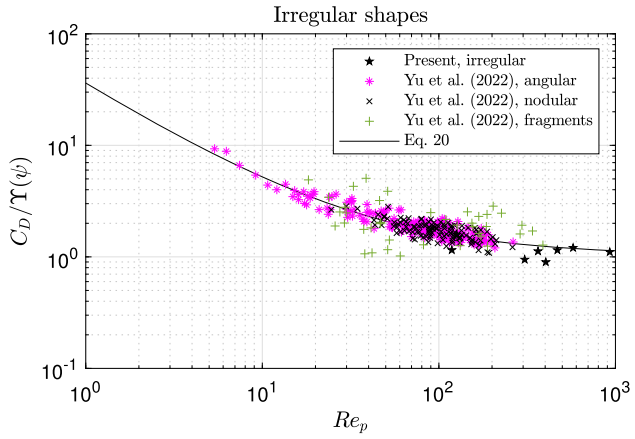

Fig. 12. Measured drag coefficients C_D, normalized by the function $\Upsilon(\psi)$, versus Reynolds number Re_p for settling irregularly-shaped microplastic particles. Note the improved clustering relative to Fig. 10.

To look for secondary dependence on ψ, we now plot $C_D/\Gamma(Re_p)$ versus ψ in Fig. 11, as suggested by Eq. (20). Interestingly, no discernible dependence on ψ is evident in the data compiled by Yu et al. (2022), generally having lower ψ. Secondary dependence on ψ is, however, evident in the irregular particles tested herein. These suggest a decreasing drag coefficient for larger ψ, which makes physical sense. To account for this secondary dependence, we therefore utilize the function

$$\Upsilon(\psi) = \min(0.44\psi^{-2}, 1) \tag{22}$$

which is depicted on Fig. 11 as the full line. Note that this function results in unity for $\psi \leq \sqrt{0.44} \approx 0.66$, and hence may be simply omitted for irregular particles in this range. The coefficient 0.44 is not chosen arbitrarily. Rather, it has been selected to match the second argument in Eq. (17), such that at the limit where Re_p is large and $\psi = 1$, Eq. (20) predicts the same C_D as for spheres.

The data is finally re-plotted as $C_D/\Upsilon(\psi)$ versus Re_p in Fig. 12, again as suggested by Eq. (20). Improved clustering of the presently tested irregularly-shaped particles relative to Fig. 10 is now clear, confirming that the secondary dependence on ψ has been reasonably accounted for.

Note that if the sphericity of an irregularly-shaped particle is unknown, it may be approximated from

$$\psi = \left(\frac{c^2}{ab}\right)^{1/3}, \tag{23}$$

as done by e.g. Kerpen et al. (2020) for the irregular microplastic particles considered in the present work, leading to the values in Table 3.

We finally wish to emphasize that, as only similar particle shape (and not material) has been assumed, there is nothing preventing application of the method developed in this sub-section based on data for microplastic particles on other particles having irregular shape e.g. natural sediment grains. This general validity is directly confirmed in Appendix A, see Fig. A.15.

5. Comparison with the predictive method of Yu et al. (2022)

Yu et al. (2022) systematically compared the accuracy of their formulation for predicting settling velocities of microplastic particles with those proposed previously by several other researchers (Song et al., 2008; Alcerreca et al., 2013; Chubarenko et al., 2016; Song et al., 2017; Waldschläger and Schüttrumpf, 2019; Wang et al., 2021; Francalanci et al., 2021). They generally demonstrated convincingly superior predictive accuracy of their method. For this reason, we will now compare

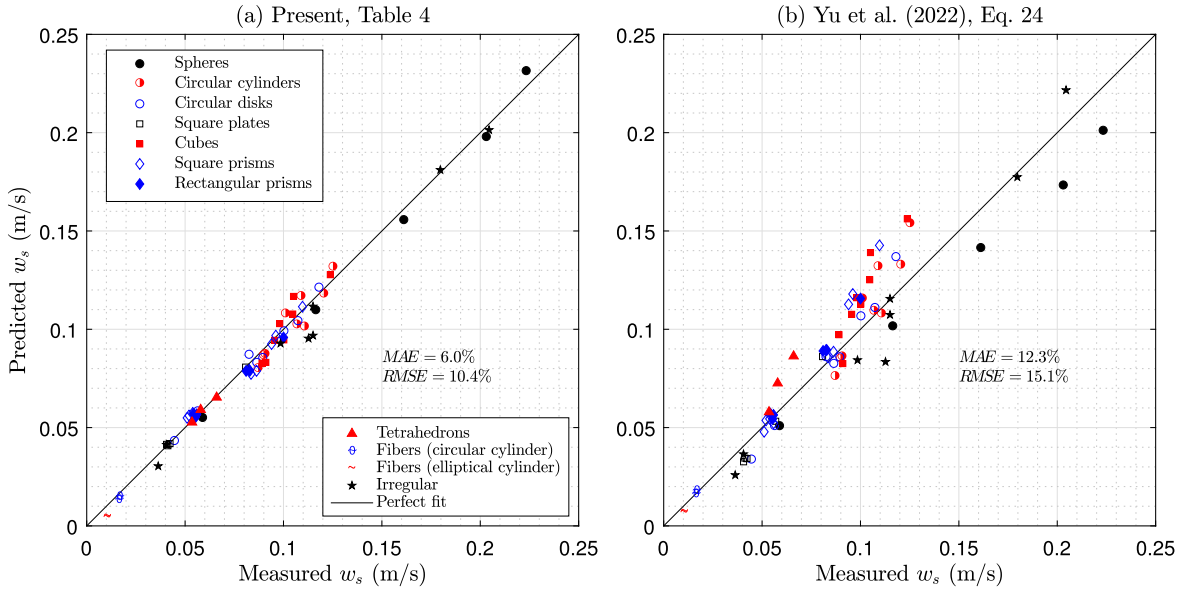

Fig. 13. Comparison of measured settling velocities (present data set) versus those predicted using (a) the present methodology, summarized in Table 4 and (b) the formulation of Yu et al. (2022), Eq. (24).

the accuracy of the present methodology, as summarized in Table 4, exclusively with that of Yu et al. (2022).

Yu et al. (2022) proposed the following general formulation for predicting the settling velocity of microplastic particles:

$$w_s = \sqrt[3]{\nu g\,(s-1)}\sqrt{\frac{4d_*}{3C_n}}, \tag{24}$$

where

$$d_* = \sqrt[3]{\frac{g\,(s-1)}{\nu^2}}\,d_n, \tag{25}$$

$$C_n = \frac{C_{d,s}}{(d_*^{\beta_1}\psi^{d_*^{\beta_2}}CSF^{d_*^{\beta_3}})^{\beta_4}}, \tag{26}$$

$$C_{d,s} = \frac{432}{d_*^3}\left(1+0.022d_*^3\right)^{0.54} + 0.47\left[1-\exp\left(-0.15d_*^{0.45}\right)\right], \tag{27}$$

$\beta_1 = -0.25$, $\beta_2 = 0.03$, $\beta_3 = 0.33$ and $\beta_4 = 0.25$.

To begin, let us consider the performance in predicting the settling velocities for the present data set, comprised of $N = 66$ particles (Tables 2 and 3). Comparison of predicted versus measured w_s values made using the present methodology is presented in Fig. 13(a). This same comparison, but based on predictions made with the formulation of Yu et al. (2022), Eq. (24), is similarly presented in Fig. 13(b).

To assess quantitative accuracy, following Yu et al. (2022), we will consider both the mean-absolute error

$$MAE = \frac{1}{N}\sum_{i=1}^{N}\frac{|P_i - O_i|}{O_i} \tag{28}$$

and the root-mean-square error

$$RMSE = \sqrt{\frac{1}{N}\sum_{i=1}^{N}\left(\frac{P_i - O_i}{O_i}\right)^2} \tag{29}$$

both defined on a relative basis. The errors above are defined generically, where P represents a prediction and O represents an observation (i.e. a measured value), with N being the sample size. As indicated in Fig. 13, the present methodology yields considerably lower errors when applied on the present data set, relative to predictions based on the formulation of Yu et al. (2022). This is perhaps not too surprising, as Yu et al. (2022) did not have access to the present data when making (and optimizing) their formulation.

Let us now similarly consider the performance on the extensive data set ($N = 699$ particles) compiled by Yu et al. (2022). Predicted versus measured w_s values are presented in Fig. 14, in the same fashion as in Fig. 13. Slightly better clustering around the line of perfect agreement is observed with the present methodology, Fig. 14(a), relative to that of Yu et al. (2022), shown in Fig. 14(b). This observation is also reflected in the reduced error measures shown in this figure. In particular, it is noted that the systematic over-prediction for many of the irregular particles observed using the Yu et al. (2022) formulation (Fig. 14b) is removed with the present methodology (Fig. 14a). Similarly, the systematic under-prediction for many of the spheres using the Yu et al. (2022) formulation is improved via the present methodology.

The predictive errors for samples divided according to both shape (combining both data sets, when relevant) or data set are summarized in Table 5, including all combined data in the final row. Here reduced errors for nearly all shapes are achieved via the present methodology, relative to the formulation of Yu et al. (2022). The lone exception is perhaps fibers, which yield a mixed result (*MAE* reduced, but *RMSE* increased). Of all the particle types considered, we expect those having spherical and irregular shapes are perhaps of most practical interest. It is seen from Table 5 that the present shape-by-shape methodology leads to increased accuracy for both.

The predictive accuracy for the settling velocity of microplastic particles achieved using the unified formulation of Yu et al. (2022) is, on the one hand, already quite impressive. On the other hand, if a particle has a known regular shape (or is irregular), there would seemingly be no reason not to take this information into account, heralding the present approach. Moreover, as the present formulation is presented in terms of an arguably more properly defined drag coefficient C_D, attempting to take into account preferential orientation observed during settling, it has the added benefit of yielding more familiar insight into the hydrodynamics of the settling process. Indeed, many of the regular shapes considered having sharp edges have resulted in simple constant C_D models (see again Table 4) for the range of Reynolds numbers considered. In each case these match closely with expectations for fixed bodies from standard fluid mechanics texts. This suggests that, for Reynolds numbers e.g. below those considered herein, drag coefficients from standard hydrodynamics tables and drag coefficient curves for fixed bodies can likely be applied for predicting the settling velocity of microplastic particles with reasonable confidence.

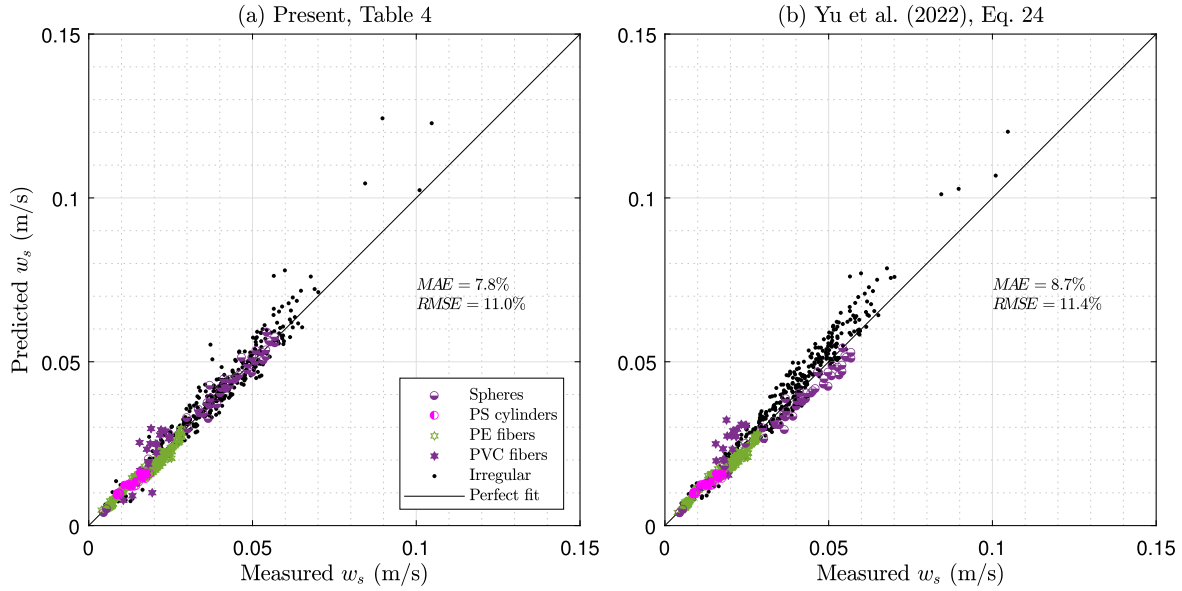

Fig. 14. Comparison of measured settling velocities (data set compiled by Yu et al., 2022) versus those predicted using (a) the present methodology, summarized in Table 4 and (b) the formulation of Yu et al. (2022), Eq. (24).

Table 5
Comparison of errors for settling velocity predictions for microplastic particles having various shapes made using the present methodology, as summarized in Table 4 and that of Yu et al. (2022), Eq. (24). Also provided are comparisons for the present data set, that compiled by Yu et al. (2022), as well as both data sets combined. The lowest errors for each sample considered are highlighted in bold.

Shape	N	Present		Yu et al. (2022)	
		MAE	*RMSE*	*MAE*	*RMSE*
Spheres	47	**4.4%**	**5.9%**	7.8%	8.8%
Cylinders	35	**7.5**	**8.6**	9.5	11.1
Circular disks	8	**3.3**	**3.6**	9.0	11.3
Square plates	5	**1.1**	**1.3**	13.7	14.9
Cubes	8	**5.6**	**6.4**	17.5	19.2
Rectangular prisms	16	**4.1**	**5.0**	9.1	12.3
Tetrahedrons	3	**1.6**	**1.6**	21.4	23.5
Fibers	263	**8.4**	12.1	8.6	**11.9**
Irregular	380	**7.9**	**11.3**	9.1	11.5
Present data	66	**6.0%**	**10.4%**	12.3%	15.1%
Yu et al. (2022) data	699	**7.8**	**11.0**	8.7	11.4
Combined data	765	**7.6**	**10.9**	9.0	11.7

It may finally be argued that the method of Yu et al. (2022) is preferable because of its simplistic use of a single set of equations. However, the two methods actually have a comparable number of fitted empirical coefficients. Inspection of Eqs. (24)–(27) reveals that the formulation of Yu et al. (2022) contains 11 independent coefficients. By comparison, all predictive equations comprising the present approach, as summarized in the second-to-last column of Table 4, involve a total of 15 independent empirical coefficients. Many (five) of these correspond simply to constant C_D values (all near unity) determined for each shape, each with strong physical basis. In summary, the two methods are comparable in terms of their total complexity. We would argue that, on a shape-by-shape basis, the present methodology for predicting settling velocities of microplastic particles is simple, elegant and seemingly accurate.

6. Summary and conclusions

The settling velocities of 66 microplastic particle groups having various shape, size and density have been experimentally measured. These include particles having regular (58) and irregular (eight) shapes. Regular shapes considered include: spheres, cylinders, circular disks, square plates, cubes, other cuboids (square and rectangular prisms), tetrahedrons, and fibers. Microplastic settling velocities for particles having many of these shapes (disks, plates, cubes, other cuboids, and tetrahedrons) have not been measured previously. The present experiments have generally considered a Reynolds number $Re_p > 10^2$, extending the range of prior studies.

Observations from these experiments have shown that settling microplastic particles have a preferential orientation, i.e. they tend to settle with their largest projection area A normal to the line of motion. This is in line with observations long known for e.g. sediment particles. On physical grounds, it has been shown that this leads to a length scale within the drag coefficient C_D, defined in Eq. (6), that is proportional to only the shortest particle dimension i.e. $d_D \sim c$. This is contrary to the prevailing convention of utilizing the nominal diameter d_n in this context.

The present experimental data for settling velocity of microplastic particles has been combined with the extensive data set recently compiled by Yu et al. (2022), and then analyzed on a shape-by-shape basis. Predictive formulations for the drag coefficients have been proposed for each shape. For shapes having sharp edges, simple constant C_D models are proposed, valid within the range of Re_p considered. These have been shown to be generally consistent with expectations based on known drag coefficients for fixed bodies. Parameterizations and predictive equations for each shape considered are summarized in Table 4.

Related to the argument above on preferential particle settling orientation, it has been shown for selected shapes that the prevailing convention of utilizing d_n, rather than d_D, in the drag coefficient can lead to increased scatter and/or false Reynolds number dependence, particularly for elongated (e.g. cylinders) or flat particles (e.g. disks and plates). Also in contrast to the prevailing convention, the length scale appearing within the Reynolds number, d_p, has been regarded as fundamentally independent of that used in C_D. For most particle shapes considered (the lone exception being combined cylinders and fibers) best results have been obtained using $d_p \sim \sqrt{ab}$, where a and b are respectively the longest and intermediate particle dimensions. This strategy elegantly leads to the numerator of the widely-used Corey (1949) shape factor ($CSF = c/\sqrt{ab}$, Eq. (2)), represented in the drag coefficient, with the denominator represented in the Reynolds number.

Predictive accuracy has been compared with the formulation of Yu et al. (2022), there established as the best of available methods published thus far. The present methodology is shown to give superior

accuracy based on the available data for nearly all shapes considered. The lone exception is fibers, where the accuracy of the two methodologies is similar. These results are summarized quantitatively in Table 5. It is also emphasized that the method developed for irregularly-shaped particles is equally-well suited for predicting the settling velocity of natural sediment grains. This is demonstrated in Appendix A below.

All experimental data newly collected in the present study are freely available at the URL indicated in the Data Availability Statement below. Selected videos showing the setting for particles representing each of the 66 particle groups considered herein are likewise provided there.

CRediT authorship contribution statement

Koray Deniz Goral: Conceptualization, Data curation, Formal analysis, Investigation, Methodology, Resources, Visualization, Writing – original draft, Writing – review & editing. **Hasan Gokhan Guler:** Conceptualization, Data curation, Funding acquisition, Investigation, Writing – review & editing. **Bjarke Eltard Larsen:** Conceptualization, Funding acquisition, Validation, Writing – review & editing. **Stefan Carstensen:** Conceptualization, Funding acquisition, Resources, Supervision, Writing – review & editing. **Erik Damgaard Christensen:** Conceptualization, Funding acquisition, Supervision, Writing – review & editing. **Nils B. Kerpen:** Conceptualization, Funding acquisition, Methodology, Resources, Writing – review & editing. **Torsten Schlurmann:** Conceptualization, Funding acquisition, Resources, Writing – review & editing. **David R. Fuhrman:** Conceptualization, Formal analysis, Funding acquisition, Methodology, Project administration, Supervision, Validation, Writing – original draft, Writing – review & editing.

Declaration of competing interest

The authors declare that they have no known competing financial interests or personal relationships that could have appeared to influence the work reported in this paper.

Data availability

The experimental data set collected in the present study is freely available at https://doi.org/10.11583/DTU.19722160. The data set provided includes the particle descriptions and properties, the time series of measured vertical particle positions, the resulting settling velocities w_s, their standard deviations σ_s, as well as example settling videos representing each of the 66 particle groups considered.

Acknowledgements

This research has been financially supported by the Independent Research Fund Denmark project MPCOAST: MicroPlastic transport processes in the COASTal environment, grant no. 0136-00227B. The second author additionally acknowledges financial support from The Scientific and Technical Research Council of Turkey (TUBITAK) under the 2219 International Postdoctoral Research Fellowship Programme. This support is greatly appreciated.

Appendix A. Application on natural sediments

In this appendix, we will demonstrate and confirm that the present methodology developed for predicting the settling velocity of irregularly-shaped microplastic particles, Eqs. (20)–(22), is equally well-suited for applications involving natural sediments. For this purpose, we will consider the data sets of Corey (1949) (representative data selected from his Figs. 3–5, Engelund and Hansen (1972) and Smith and Cheung (2002), from which the necessary information is provided directly or can be reasonably approximated.

Corey (1949) and Smith and Cheung (2002) report sediment grain dimensions a, b and c directly, hence requiring no approximations

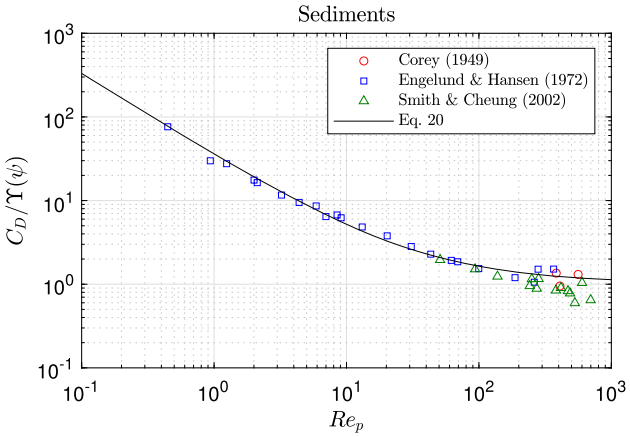

Fig. A.15. Measured drag coefficients C_D, normalized by the function $\Upsilon(\psi)$, versus Reynolds number Re_p for settling sediment grains. Note the similar match as for irregularly-shaped microplastic particles, presented in Fig. 12.

for these and other derived quantities. Engelund and Hansen (1972) report both nominal diameter d_n and sieve diameter d_s. Other quantities for their particles have therefore been estimated as follows: Smith and Cheung (2002) directly report (see their Fig. 4) the typical ratio $b/d_s = 1.2$. From inspection of their Table 1, we similarly find the mean ratio $b/c = 1.47$. Combining these yields the approximation $c/d_s = 0.82$, which has been assumed typical and used to estimate c for the Engelund and Hansen (1972) data set. This then leads naturally to $ab = d_n^3/c$, such that both $d_D = c$ and $d_p = \sqrt{ab}$ (hence C_D and Re_p) can be estimated as indicated for irregular particles in Table 4. For all three sediment data sets, the sphericity has been estimated using Eq. (23). All other properties are taken either as directly reported in the original references, or based on the reported water temperatures.

Results for the experimentally measured settling velocities for these sediments are presented in Fig. A.15. This figure maintains identical fashion as Fig. 12 for irregularly-shaped microplastic particles. A generally excellent match with Eq. (20) is observed in Fig. A.15, especially for the data sets of Corey (1949) and Engelund and Hansen (1972). The considered data collectively span the range $4 \times 10^{-1} \leq Re_p \leq 10^3$. This extends the lower end tested by an order of magnitude relative to the microplastic particles considered in Fig. 12, and this lower limit is reflected in Table 4. The data of Smith and Cheung (2002) match reasonably, but are systematically below the curve. This discrepancy is likely in part due to uncertainty in the individual sediment grain densities. In the calculations above, we have utilized their reported mean value $\rho_p = 2550$ kg/m^3. It must be noted, however, that they reported calculated densities spanning a wide range 2180–2970 kg/m^3, but did not specify these on a grain-by-grain basis. The errors using Eq. (20) to predict w_s for the three combined sediment data sets ($N = 39$ samples) correspond to $MAE = 10.0\%$ and $RMSE = 12.3\%$, with a significant portion of the error stemming from the Smith and Cheung (2002) data. If a sample with size $N = 25$, comprised of only the selected Corey (1949) and Engelund and Hansen (1972) data, is instead used then the errors reduce to $MAE = 7.3\%$ and $RMSE = 8.6\%$. These are comparable to (actually slightly lower than) those achieved for irregularly-shaped microplastic particles in Table 5.

Eqs. (20)–(22) have been developed based exclusively on fitting data for settling irregularly-shaped microplastic particles, see Figs. 10–12. Nevertheless, that this method seemingly works equally well for natural sediments is not surprising. This should, in fact, be expected from dimensional analysis of this problem, leading to Eq. (13). This predicts that particles having common shape (or in this case, common characterization as irregularly shaped) ought to have unique Reynolds number dependence. This further application considering the settling velocity of natural sediment grains demonstrates this concept nicely.

References

Ahrens, J.P., 2000. A fall-velocity equation. J. Waterw. Port Coast. Ocean Eng. 126, 99–102. https://doi.org/10.1061/(ASCE)0733-950X(2000)126:2(99).

Alcerreca, J.C., Silva, R., Mendoza, E., 2013. Simple settling velocity formula for calcareous sand. J. Hydraul. Res. 51, 215–219. https://doi.org/10.1080/00221686.2012.753645.

Alsina, J., Jongedijk, C., van Sebille, E., 2020. Laboratory measurements of the wave-induced motion of plastic particles: influence of wave period, plastic size and plastic density. J. Geophys. Res., Oceans 125 (12), e2020JC016294. https://doi.org/10.1029/2020JC016294.

Barnes, D., Galgani, F., Thompson, R., Barlaz, M., 2009. Accumulation and fragmentation of plastic debris in global environments. Philos. Trans. R. Soc. B 364, 1985–1998. https://doi.org/10.1098/rstb.2008.0205.

Brewer, A., Dror, I., Berkowitz, B., 2021. The mobility of plastic nanoparticles in aqueous and soil environments: a critical review. ACS ES&T Water 1, 48–57. https://doi.org/10.1021/acsestwater.0c00130.

Browne, M., Crump, P., Niven, S., Teuten, E., Tonkin, A., Galloway, T., Thompson, R., 2011. Accumulation of microplastic on shorelines worldwide: sources and sinks. Environ. Sci. Technol. 45, 9175–9179. https://doi.org/10.1021/es201811s.

Camenen, B., 2007. Simple and general formula for the settling velocity of particles. J. Hydraul. Eng. 133, 229–233. https://doi.org/10.1061/(ASCE)0733-9429(2007)133:2(229).

Chee, S., Myllys, N., Barsanti, K.C., Wong, B.M., Smith, J.N., 2019. An experimental and modeling study of nanoparticle formation and growth from dimethylamine and nitric acid. J. Phys. Chem. A 123, 5640–5648. https://doi.org/10.1021/acs.jpca.9b03326.

Chubarenko, I., Bagaev, A., Zobkov, M., Esiukova, E., 2016. On some physical and dynamical properties of microplastic particles in marine environment. Mar. Pollut. Bull. 108, 105–112. https://doi.org/10.1016/j.marpolbul.2016.04.048.

Corey, A.T., 1949. Influence of shape on the fall velocity of sand grains. Master's thesis. Colorado Agricultural and Mechanical College. https://hdl.handle.net/10217/195976.

Cozar, A., Echevarria, F., Gonzalez-Gordillo, I., Irigoien, X., Ubeda, B., Hernandez-Leon, S., Palma, A., Navarro, S., de Lomas, J.G., Ruiz, A., de Puelles, M.F., Duarte, C., 2014. Plastic debris in the open ocean. Proc. Natl. Acad. Sci. USA 111 (28), 10239–10244. https://doi.org/10.1073/pnas.1314705111.

Dietrich, W.E., 1982. Settling velocity of natural particles. Water Resour. Res. 18, 1615–1626. https://doi.org/10.1029/WR018i006p01615.

Engelund, F., Hansen, E., 1972. A Monograph on Sediment Transport in Alluvial Streams. Technical Press, Copenhagen.

Ferguson, R., Church, M., 2004. A simple universal equation for grain settling velocity. J. Sediment. Res. 74, 933–937. https://doi.org/10.1306/051204740933.

Francalanci, S., Paris, E., Solari, L., 2021. On the prediction of settling velocity for plastic particles of different shapes. Environ. Pollut. 290, 118068. https://doi.org/10.1016/j.envpol.2021.118068.

Fredsøe, J., Deigaard, R., 1992. Mechanics of Coastal Sediment Transport. World Scientific.

Goral, K.D., Guler, H.G., Baykal, C., Yalciner, A.C., 2021. An experimental study on the motion of solid spheres under solitary wave attack. Ocean Eng. 240, 109946. https://doi.org/10.1016/j.oceaneng.2021.109946.

Guler, H.G., Larsen, B.E., Quintana, O., Goral, K.D., Carstensen, S., Christensen, E.D., Kerpen, N.B., Schlurmann, T., Fuhrman, D.R., 2022. Experimental study of non-buoyant microplastic transport beneath breaking irregular waves on a live sediment bed. Mar. Pollut. Bull. 181, 113902. https://doi.org/10.1016/j.marpolbul.2022.113902.

ISO, 2012. Plastics – Methods for Determining the Density of Noncellular Plastics – Part 1: Immersion Method, Liquid Pyknometer Method and Titration Method. Standard ISO 1183-1. International Organization for Standardization, Geneva, CH.

Jambeck, J.R., Geyer, R., Wilcox, C., Siegler, T.R., Perryman, M., Andrady, A., Narayan, R., Law, K.L., 2015. Plastic waste inputs from land into the ocean. Science 347, 768–771. https://doi.org/10.1126/science.1260352.

Kerpen, N.B., Schlurmann, T., Schendel, A., Gundlach, J., Marquard, D., Hüpgen, M., 2020. Wave-induced distribution of microplastic in the surf zone. Front. Mar. Sci. 7, 979. https://doi.org/10.3389/fmars.2020.590565.

Khatmullina, L., Chubarenko, I., 2021. Thin synthetic fibers sinking in still and convectively mixing water: laboratory experiments and projection to oceanic environment. Environ. Pollut. 288, 117714. https://doi.org/10.1016/j.envpol.2021.117714.

Khatmullina, L., Isachenko, I., 2017. Settling velocity of microplastic particles of regular shapes. Mar. Pollut. Bull. 114, 871–880. https://doi.org/10.1016/j.marpolbul.2016.11.024.

Kowalski, N., Reichardt, A.M., Waniek, J.J., 2016. Sinking rates of microplastics and potential implications of their alteration by physical, biological, and chemical factors. Mar. Pollut. Bull. 109, 310–319. https://doi.org/10.1016/j.marpolbul.2016.05.064.

Lamb, J., Willis, B., Fiorenza, E., Couch, C., Howard, R., Rader, D., True, J., Kelly, L., Ahmad, A., Jompa, J., Harvell, C., 2018. Plastic waste associated with disease on coral reefs. Science 359, 460–462. https://10.1126/science.aar3320.

Law, K., Thompson, R., 2014. Microplastics in the seas. Science 345, 144–145. https://doi.org/10.1126/science.1254065.

Mendrik, F., Fernández, R., Hackney, C., Waller, C., Parsons, D., 2023. Non-buoyant microplastic settling velocity varies with biofilm growth and ambient water salinity. Commun. Earth Environ. 4. https://doi.org/10.1038/s43247-023-00690-z.

Nerland, I., Halsband, C., Allan, I., Thomas, K., 2014. Microplastics in Marine Environments: Occurrence, Distribution and Effects. Technical Report 6754-2014. Oslo: Norwegian Institute for Water Research.

Nguyen, T.H., 2021. Settling behaviour of irregular-shaped polystyrene microplastics. VNUHCM J. Eng. Technol. 4, 1229–1238. https://doi.org/10.32508/stdjet.v4i4.905.

Nguyen, T.H., Kieu-Le, T.C., Tang, F.H., Maggi, F., 2022. Controlling factors of microplastic fibre settling through a water column. Sci. Total Environ. 838, 156011. https://doi.org/10.1016/j.scitotenv.2022.156011.

Nguyen, T.H., Tang, F.H.M., Maggi, F., 2020. Sinking of microbial-associated microplastics in natural waters. PLoS ONE 15, 1–20. https://doi.org/10.1371/journal.pone.0228209.

Peeken, I., Primpke, S., Beyer, B., Gütermann, J., Katlein, C., Krumpen, T., Bergmann, M., Hehemann, L., Gerdts, G., 2018. Arctic sea ice is an important temporal sink and means of transport for microplastic. Nat. Commun. 9, 1505. https://10.1038/s41467-018-03825-5.

Petersen, B.H., 2006. Hydraulik - Stationære strømninger. Polyteknisk Forlag (in Danish).

Roberson, J.A., Crowe, C.T., 1993. Engineering Fluid Mechanics, fifth ed. John Wiley & Sons.

Rubey, W.W., 1933. Settling velocities of gravel, sand, and silt particles. Am. J. Sci. 25, 325–328.

Schiller, L., Naumann, Z., 1935. A drag coefficient correlation. Z. Ver. Dtsch. Ing. 77, 318–320.

Smith, D.A., Cheung, K.F., 2002. Empirical relationships for grain size parameters of calcareous sand on Oahu, Hawaii. J. Coast. Res. 18, 82–93.

Song, X., Xu, Z., Li, G., Pang, Z., Zhu, Z., 2017. A new model for predicting drag coefficient and settling velocity of spherical and non-spherical particle in Newtonian fluid. Powder Technol. 321, 242–250. https://doi.org/10.1016/j.powtec.2017.08.017.

Song, Z., Wu, T., Xu, F., Li, R., 2008. A simple formula for predicting settling velocity of sediment particles. Water Sci. Eng. 1, 37–43. https://doi.org/10.3882/j.issn.1674-2370.2008.01.005.

Soulsby, R., 1997. Dynamics of Marine Sands. Thomas Telford Publishing.

Stokes, G.G., 1851. On the Effect of the Internal Friction of Fluids on the Motion of Pendulums. Transactions of the Cambridge Philosophical Society, vol. 9, p. 8.

Van Melkebeke, M., Janssen, C., De Meester, S., 2020. Characteristics and sinking behavior of typical microplastics including the potential effect of biofouling: implications for remediation. Environ. Sci. Technol. 54, 8668–8680. https://doi.org/10.1021/acs.est.9b07378.

van Sebille, E., Wilcox, C., Lebreton, L., Maximenko, N., Hardesty, B., van Franeker, J., Eriksen, M., Siegel, D., Galgani, F., Law, K., 2015. A global inventory of small floating plastic debris. Environ. Res. Lett. 10, 124006. https://doi.org/10.1088/1748-9326/10/12/124006.

Wadell, H., 1935. Volume, shape, and roundness of quartz particles. J. Geol. 43, 250–280.

Waldschläger, K., Born, M., Cowger, W., Gray, A., Schüttrumpf, H., 2020. Settling and rising velocities of environmentally weathered micro- and macroplastic particles. Environ. Res. 191, 110192. https://doi.org/10.1016/j.envres.2020.110192.

Waldschläger, K., Schüttrumpf, H., 2019. Effects of particle properties on the settling and rise velocities of microplastics in freshwater under laboratory conditions. Environ. Sci. Technol. 53, 1958–1966. https://doi.org/10.1021/acs.est.8b06794.

Wang, Z., Dou, M., Ren, P., Sun, B., Jia, R., Zhou, Y., 2021. Settling velocity of irregularly shaped microplastics under steady and dynamic flow conditions. Environ. Sci. Pollut. Res. 28, 1–17. https://doi.org/10.1007/s11356-021-14654-3.

Wieczorek, A., Morrison, L., Croot, P., Allcock, A., MacLoughlin, E., Savard, O., Brownlow, H., Doyle, T., 2018. Frequency of microplastics in mesopelagic fishes from the northwest Atlantic. Front. Mar. Sci. 5, 39. https://10.3389/fmars.2018.00039.

Willmarth, W.W., Hawk, N.E., Harvey, R.L., 1964. Steady and unsteady motions and wakes of freely falling disks. Phys. Fluids 7, 197–208. https://doi.org/10.1063/1.1711133.

Yu, Z., Yang, G., Zhang, W., 2022. A new model for the terminal settling velocity of microplastics. Mar. Pollut. Bull. 176, 113449. https://doi.org/10.1016/j.marpolbul.2022.113449.

Zhiyao, S., Tingting, W., Fumin, X., Ruijie, L., 2008. A simple formula for predicting settling velocity of sediment particles. Water Sci. Eng. 1, 37–43. https://doi.org/10.1016/S1674-2370(15)30017-X.